Cement & Concrete Composites 38 (2013) 12–20

Contents lists available at SciVerse ScienceDirect

Cement & Concrete Composites

journal homepage: www.elsevier.com/locate/cemconcomp

Durability of very high volume fly ash cement pastes and mortars in aggressive solutions

Shane Donatello *, Angel Palomo, Ana Fernández-Jiménez

Eduardo Torroja Institute of Construction Sciences (CSIC), Calle Serrano Galvache 4, 28033 Madrid, Spain

ARTICLE INFO

Article history:
Received 3 January 2013
Received in revised form 8 February 2013
Accepted 6 March 2013
Available online 18 March 2013

Keywords:
Durability
Sodium sulfate
Sea water
Acid
Fly ash
Cement

ABSTRACT

The resistance of very high volume fly ash cement pastes and mortars activated by Na_2SO_4 has been monitored following immersion for up to 90 d in 0.1 M HCl, 4.4% Na_2SO_4 and ASTM-compliant sea water. Changes in the compressive strengths of mortars and in crystalline phases, bond environments, and the microstructure of pastes following immersion were monitored. Experiments were repeated with a commercially available sulfate resistant cement. Both cements were found to present adequate resistance to both sea water and the Na_2SO_4 solution. However, both were severely degraded by acid immersion. Differences in potential degradation mechanisms based on the chemistry of the fly ash binder and the reference cement are discussed.

1. Introduction

Despite the fact that concrete is a fundamental component of modern infrastructure, its durability can be a major problem affecting the lifespan of structures and involving significant repair costs. For example, in the US alone, the total cost of concrete repair, rehabilitation and protection was estimated to be around $18–21 billion in 2006 [1]. While poor workmanship is a highly significant factor in real-life examples, from an academic point of view, of greater interest are the chemical mechanisms of concrete degradation. The sand and aggregate used in concrete are generally inert, so long as they do not contain reactive silica species [2–4]. Therefore, chemical degradation tends to involve an attack on portlandite and the other reaction products formed during Portland cement (PC) hydration.

The partial replacement of PC with pozzolanic materials, generally from 5% to 30% by mass, has been shown to improve the durability properties of blended cements [5–7]. This is largely attributed to the pozzolanic reaction, where reactive siliceous and aluminous phases react with portlandite to form new C-S-H or C-AS-H type phases, provoking a refinement in the pore structure and thus impeding the penetration and movement of potentially aggressive ions such as H^+, Cl^- and SO_4^{2-} [8].

Importantly, the replacement of PC with pozzolans reduces the overall CO_2 footprint of the material. Emissions of CO_2 are an important consideration in cement production since, due to its sheer scale, the industry accounts for 5–8% of global anthropogenic emissions [9].

The most widely used cement replacement material is coal combustion fly ash (FA). In the EU, replacement of up to 35% of PC with FA is permitted for a range of cement types and in one case up to 55% is specified [10]. However, the pozzolanic reaction with FA is slow and often causes a significant decrease in early-age compressive strengths. These effects have effectively limited FA replacement rates to the 55% currently specified in EN 197-1 in what are generally termed "high volume fly ash (HVFA) cements" [11–14]. One potential method of compensating for the reduction in early strength in fly ash blended cements is to incorporate fine limestone, which is known to increase early strengths [14–17]. Such ternary hybrid cements may offer synergistic effects in terms of early and later strength development and can meet European compositions specified in EN 197-1 [10].

However, limestone does not necessarily provide significant alkalinity that is lost when lowering the cement clinker content. Attempts to overcome the limited alkalinity of high volume fly ash cements have led to investigations into what can be termed "hybrid alkaline cements", where Portland cement is in a large part replaced by supplementary cementitious materials such as blast furnace slag [18,19] or fly ash [11–14,20]. To be considered as a hybrid "alkaline" cement, it is important to include a suitable source of alkali, usually as a soluble Na compound [21]. These hybrid alkaline cements can be expected to produce a combination of different types of gels of the types C-S-H [22], C-AS-H [23,24] and N-A-S-H

* Corresponding author. Tel.: +34 913020440.
E-mail address: shanedonatello@ietcc.csic.es (S. Donatello).

0958-9465/$ - see front matter © 2013 Elsevier Ltd. All rights reserved.
http://dx.doi.org/10.1016/j.cemconcomp.2013.03.001

[25]. The possible compatibility of such gels has been studied recently in simplified systems [26,27].

Recent work published by the authors has investigated the potential of Na_2SO_4 as an activator of PC–FA blends containing very high levels of FA (ca. 80%wt.) [28]. Results clearly showed that hydration reactions, compressive strengths and gel formation were enhanced when Na_2SO_4 was used as an activator. Despite the promising initial results with such blends and the associated CO_2 footprint reductions that they would provide, it is necessary to investigate the longer term durability aspects of this "very high volume fly ash" hybrid alkaline cement.

Given that acid, seawater and sulfate attack are widely studied chemical degradation mechanisms in PC-based materials [29,30], the objective of this research was to investigate the resistance of the novel binder to immersion under these three conditions.

2. Materials and methods

2.1. Paste and mortar preparation

The hybrid cement binder (FAN-4) consisted of approximately 80% by dry mass FA and 20% by mass PC clinker (cement only with no added calcium sulfate) ground together with a small quantity of anhydrous Na_2SO_4. Further details can be found in Donatello et al. [28]. As a reference, a commercially available cement blend (MS) was also tested under the same conditions as used with the hybrid alkaline cement. Both anhydrous cements were analysed by X-ray fluorescence (Philips PW 1404/00/01) to determine major elements present and the results are given in Table 1. The MS cement was a sulfate resistant Type II Portland cement [10] containing unspecified minor additions of blastfurnace slag, other pozzolanic materials, and limestone filler. The minimum possible *w/b* (water to binder) ratios to achieve standard consistency in pastes without the addition of high range water reducers were 0.32 and 0.36 for the MS and FAN-4 pastes, respectively. Taking into account the specific gravity of the dry cements, the water volume fractions of the pastes were 49.5% (FAN-4) and 47.9% (MS). With 3:1 mortars, a fixed *w/b* ratio of 0.45 was sufficient to achieve standard flowability [31]. Standard sand [32] with a specific gravity of 2.66 was used in the preparation of all mortars. The liquid volume ratios in both sets of mortar were 22.9% (FAN-4) and 23.3% (MS).

Cement pastes and mortars were mixed according to EN 196–1 [32] and cast into 3 cm cubic stainless steel molds. After casting, the molds were placed in a humidity chamber maintained at 23 °C and >95% relative humidity. Compressive strengths (Ibertest Autotest 200/10/SW) of mortars were tested after 2 d, 7 d, and 28 d curing.

2.2. Preparation of aggressive solutions

Batches of approximately 0.1 M HCl solution were prepared by the dilution of 171 ml of 36% HCl (specific gravity of 1.18) to a final volume of 20 L with deionised water. The 4.4% Na_2SO_4 solution was prepared by the addition of 880 g of anhydrous Na_2SO_4 salt (Panreac) to 20 L of deionised water and mixing for approximately 30 min or until all of the salt had dissolved. The preparation of ASTM seawater was followed according to ASTM D1141 [33], except that in some cases hydrated salts were used instead of anhydrous ones and the weights adjusted accordingly. All salts were of laboratory or analytical grade.

Table 1
Major element composition determined by XRF (expressed as oxides in wt.%).

	SiO_2	Al_2O_3	CaO	Fe_2O_3	MgO	Na_2O	K_2O	SO_3	LOI[a]	SG[b]
FAN-4	48.7	17.1	13.5	7.4	1.8	1.8	2.1	2.2	4.4	2.58
MS	26.3	6.8	46.6	2.5	4.8	1.0	1.0	6.4	4.0	2.87

[a] LOI represents weight "loss on Ignition" at 1000 °C during 1 h in Pt crucibles.
[b] SG = specific gravity (g/cm^3) measured in a Le Chatelier flask using 2-Propanol.

2.3. Immersion in aggressive solutions

After reaching 28 d of age, the mortars were immersed in plastic containers containing one of the aforementioned solutions. In each container, 4 individual 3 cm mortar or paste cubes were placed and 2.16 L of solution added. The volume of solution was chosen to represent a volume to sample surface area ratio of 10 cm (see Eq. (1)), in accordance with the static leaching test procedure ANSI/ANS 16.1 [34]. If each face of the 3 cm cube represents 9 cm^2, each cube has a total area of 54 cm^2, and 4 cubes would total 216 cm^2.

$$\text{Ratio (cm)} = \text{Volume (2160 cm}^3\text{)/sample area (216 cm}^2\text{)} = 10\ \text{cm} \quad (1)$$

To reduce the static nature of the test, the solutions were replaced with fresh solution at the following intervals: 1 d, 2 d, 4 d, 7 d, 28 d, 56 d and 90 d.

2.4. Analysis of immersed mortars/pastes

Mortar samples were removed after 7 d, 28 d, 56 d, or 90 d of immersion, photographed, weighed, and then tested for compressive strength. Due to the high dilution of cementitious phases in mortars, immersion tests were repeated with pastes. After 7 d, 28 d, 56 d, and 90 d immersion, pastes were removed, dried, ground and further hydration reactions quenched by immersion in acetone for 5 min, removing liquid from the slurry via vacuum filtration and then repeating the procedure with ethanol. Solids were dried in a desicator for at least 24 h. The dried powders were subsequently analysed by XRD (Bruker D8 Advance) and FTIR spectroscopy (Thermo Scientific Nicolet 6700). Analysis of paste fragments from selected samples was also carried out by Field Emission SEM/EDX (Hitachi S-4800).

3. Results

3.1. Compressive strength development

Strengths for FAN-4 and MS mortars immediately prior to immersion (i.e. after 28 d curing) were 37.2 MPa and 54.1 MPa, respectively. By normalising these strengths to 100%, comparable trends in mortar compressive strengths during immersion in 4.4% Na_2SO_4, 0.1 M HCl, or the ASTM seawater are given in Fig. 1.

From the data in Fig. 1, it was clear that the 0.1 M HCl solution is highly aggressive and caused a breakdown in the sample microstructure of both groups of mortars. Although the MS mortar presents a higher initial resistance to acid, after 90 d immersion, compressive strengths were reduced by 85–90% in both sets of mortars.

In the 4.4% Na_2SO_4 solution, a completely different trend was noted. Both mortars actually gained strength during immersion. Gains were steadier and somewhat higher in the reference MS mortar although after 90 d immersion both mortars showed strength gains of around 25% relative to their strengths prior to immersion. Although seawater is also rich in SO_4^{2-}, a somewhat different trend was noticed, where the FAN-4 mortars showed steadier behaviour with a gradual increase throughout the test period. In contrast, the reference MS mortar showed an initial sharp gain in strength and then a slow gradual decrease. Regardless, all seawater immersed mortars showed net gains in compressive strength after immersion for all periods tested.

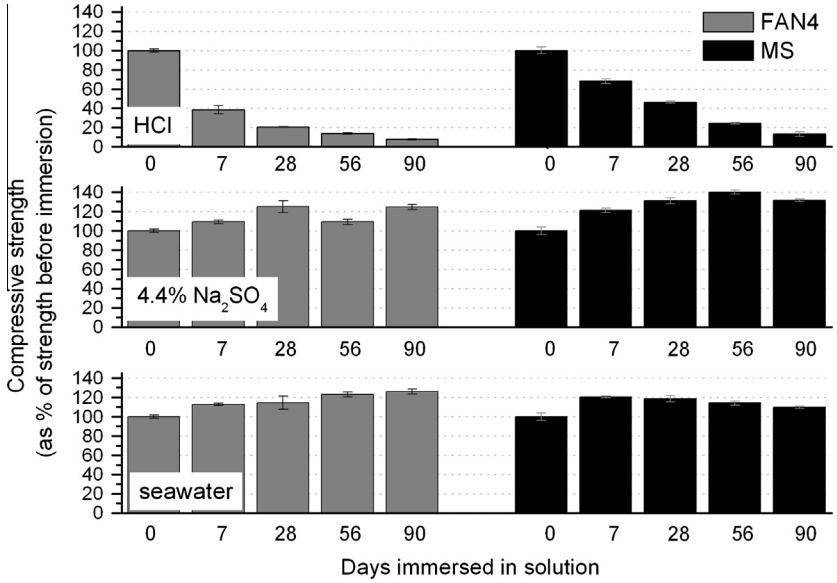

Fig. 1. Percentage changes in compressive strengths of FAN-4 and MS mortars following immersion in 0.1 M HCl, 4.4% Na_2SO_4 or ASTM compliant seawater. Values are averages of 3 measurements ± 1 standard deviation.

3.2. Changes in paste chemistry and microstructure during acid immersion

The crystalline phases present in anhydrous cements, 28 d hydrated pastes prior to immersion, and of pastes following immersion for 90 d in 0.1 M HCl are presented in Fig. 2 below.

The data in Fig. 2 show that the anhydrous MS cement was very similar to a typical PC with the main clinker phases alite, belite, tricalcium aluminate and brownmillerite all being present, as well as gypsum. The presence of minor additions is evident via the small quartz peak in anhydrous MS cement at around 27° 2Θ and the significant calcite peak at 29° 2Θ. The hydration of the paste over 28 d resulted in the complete disappearance of gypsum, a large reduction in clinker phase peaks, and the emergence of new peaks for ettringite and portlandite. After 90 d immersion in 0.1 M HCl, portlandite, ettringite and calcite contents were greatly reduced in MS pastes. A new peak at 11.2° fits perfectly with Friedeĺs salt [35] and the peak at 9.8° fits well with the main peak of synthetic AFm phases reported by Baur et al. [36] and Hirao et al. [37]. Thus the XRD presented for MS pastes suggests a conversion of AFt(SO_4) → AFm(SO_4) → AFm(Cl) (Friedels salt) during HCl immersion. Furthermore, the emergence of a background halo between 20 and 25° 2Θ after acid exposure was also observed.

In the anhydrous FAN-4 paste, phases are dominated by alite and belite from the clinker component and quartz, hematite, anorthite and maghemite from the fly ash component. Peaks

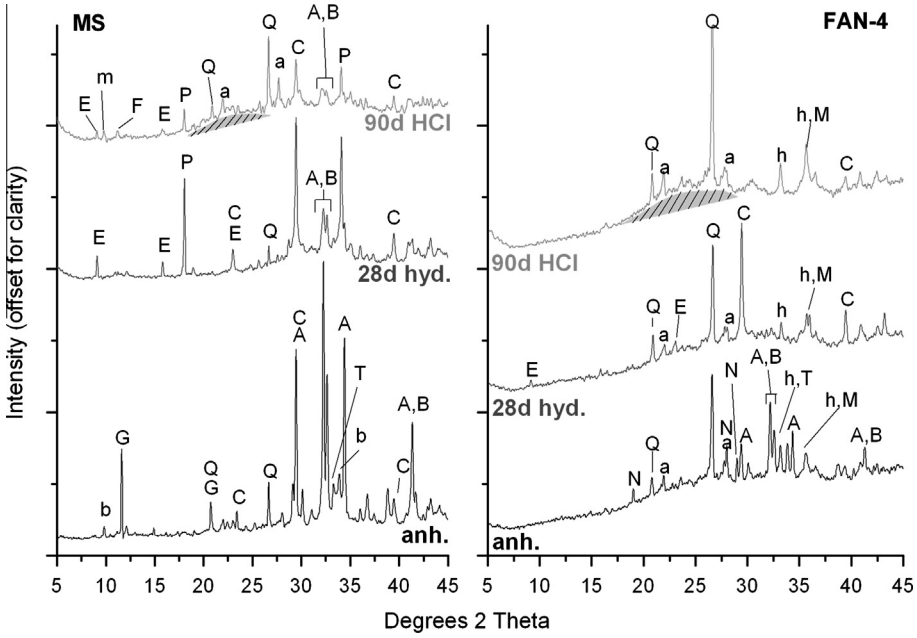

Fig. 2. XRD data of anhydrous cements, 28 d hydrated pastes prior to immersion and of pastes that had been submerged in 0.1 M HCl for 90 d. Peak labels are as follows: A – alite ($3CaO{\cdot}SiO_2$), a – anorthite ($CaAl_2Si_2O_8$), B – belite ($2CaO{\cdot}SiO_2$), b – brownmillerite ($Ca_2Al_2Fe_2O_{10}$), C – calcite ($CaCO_3$), E – ettringite ($3CaO{\cdot}Al_2O_3{\cdot}3CaSO_4{\cdot}26H_2O$), F – Friedel's salt ($3CaO{\cdot}Al_2O_3{\cdot}CaCl_2{\cdot}10H_2O$), G – gypsum ($CaSO_4{\cdot}2H_2O$), h – hematite ($Fe_2O_3$), M – maghemite ($Fe_2O_3$), m – AFm phase ($3CaO{\cdot}Al_2O_3{\cdot}CaSO_4{\cdot}12H_2O$), N – Na_2SO_4 ,P – portlandite ($Ca(OH)_2$), Q – quartz (SiO_2) and T – tri-calcium aluminate ($3CaO{\cdot}Al_2O_3$).

corresponding to the Na_2SO_4 activator were also evident. Unlike with MS pastes, after 28 d hydration, no portlandite, and only small amounts of ettringite, were detected. Significant carbonation was evident via a dominant peak for calcite at 29°. After 90 d acid immersion of FAN-4 pastes, peaks due to ettringite and calcite disappear and a significant increase in the background halo between 18 and 28° 2Θ was observed.

Both MS and FAN-4 pastes showed a common behaviour in the development of an amorphous background halo during acid immersion. To investigate this further, changes in general bond environments as demonstrated by FTIR analysis are shown in Fig. 3.

From the data in Fig. 3, it is clear that a number of important changes have taken place in bond environments that absorb within the 900–1300 cm^{-1} frequency range. This range corresponds to numerous possible bond environments such as Si–O in C-S-H type gel, quartz, silica gel and SO_4 in ettringite, gypsum and Na_2SO_4. Therefore, it was decided to subtract the spectra of pastes before and after immersion in HCl for 90 d using the OMNIC program that is used with the FTIR spectrometer. The subtracted spectra clearly highlight any gains or losses in absorption bands following acid immersion and are shown in Fig. 4.

The subtracted FTIR spectra support the XRD observations regarding the loss of portlandite and calcite in the MS paste and of calcite in the FAN-4 paste. The enhanced absorption bands at 468, 780–800 and 1080 cm^{-1} are typical bands for quartz, and also agree with the XRD observations that imply enrichment of this acid insoluble crystalline phase. A new FTIR absorption band at 1201 cm^{-1} can also be observed in both paste systems. This absorption band is typical of Si-O environments in amorphous silica gels [38–40] and corresponds well with the background halos observed in the corresponding XRD data.

The subtracted data also reveals interesting information about the loss of absorption bands that correspond to the cementitious gel phase. In the MS paste, a loss of absorption centred at 948 cm^{-1} was noted, while with the FAN-4 pastes, an absorption band centred at 981 cm^{-1} disappeared. Such an observation

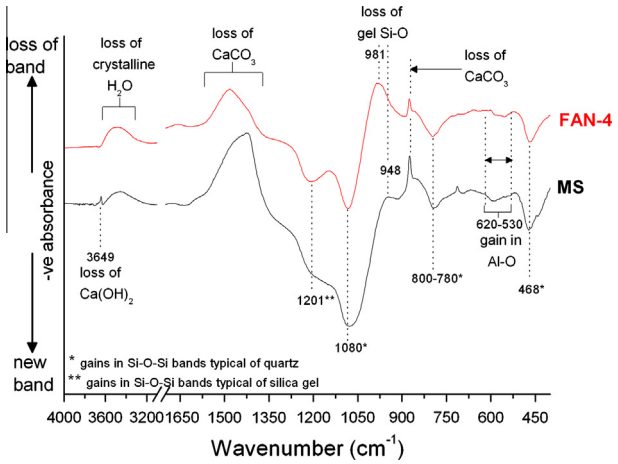

Fig. 4. Result of subtracting non-HCl immersed spectra from HCl immersed spectra for FAN-4 and MS pastes.

suggests that the gels were different in normal pastes prior to acid immersion. Finally, some changes in the 610–530 cm^{-1} range, considered to correspond to Al-O bond environments [41] were noted. These may be related to ettringite decomposition products.

Due to the major changes in both physical and chemical aspects of pastes during acid immersion, it was decided to analyse acid immersed samples by SEM/EDX. Selected images from SEM/EDX analysis of both MS and FAN-4 pastes after immersion in HCl for 90 d are included in Figs. 5 and 6, respectively.

The MS paste fragment contained areas that had been attacked by HCl to varying degrees. The most obvious signs of this were observed in paste pores. For example, in Fig. 5a, a pore containing portlandite and ettringite is clearly shown. These products are readily prone to acid attack and their existence implies that this area has not yet been sufficiently attacked. The gel around the pore in Fig. 5a has a relatively high Ca:Si ratio. In

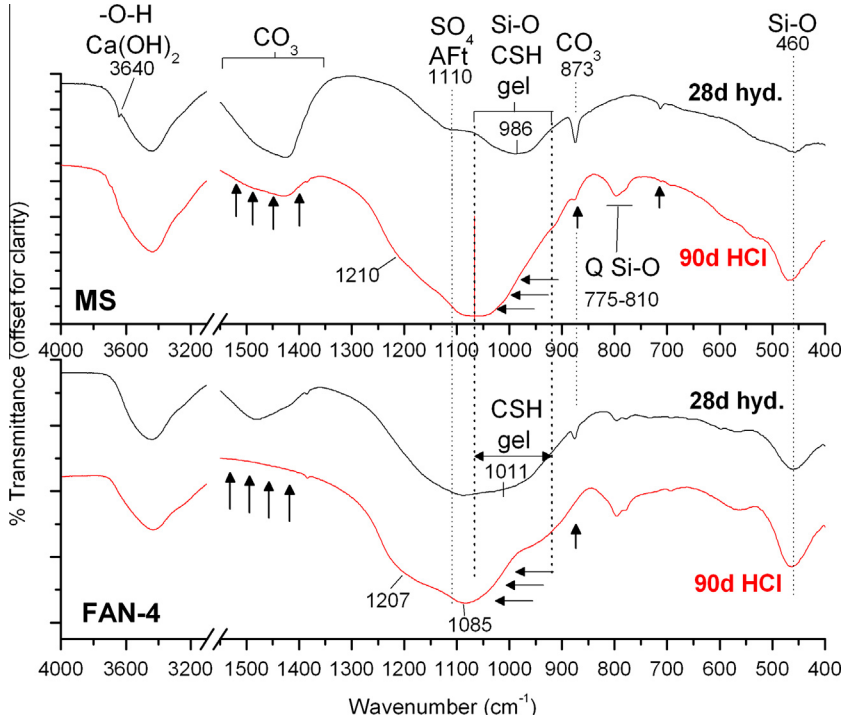

Fig. 3. Comparison of MS and FAN-4 paste FTIR data before and after immersion in acid for 90 d. Arrows indicate general losses in absorption bands following acid immersion.

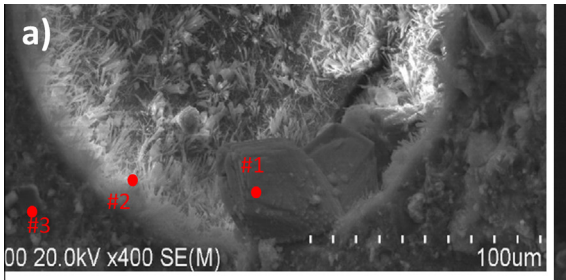

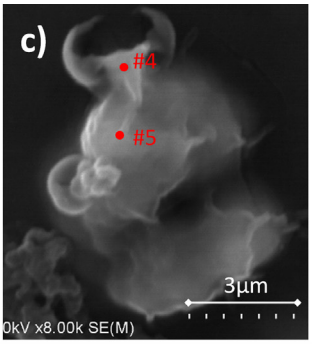

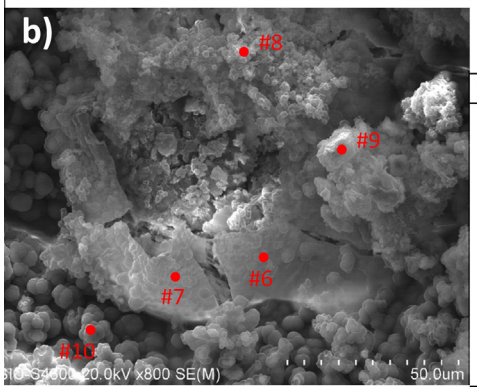

Point no.	O	Si	Al	Ca	Fe	S	K
1 (CH)	51.2	0.8		47.1		0.9	
2 (Aft)	61.4	4.1	6,6	20.1		7.7	
3 (gel)	58.7	15.6	2.6	20.5	0.7	0.3	0.4
4 (Gib)	63.5	4.6	24.6	0.5	1.7	5.1	0.1
5 (Gib)	63.6	6.1	24.1	0.5	1.1	4.5	0.1
6 (gel)	60.4	14.1	10.9	7.3	6.0	0.8	0.6
7 (gel)	60.9	13.0	13.7	6.3	4.5	1.1	0.5
8	61.4	9.8	7.7	5.6	10.2	4.7	0.5
9	63.8	25.2	6.2	0.8	2.6		1.4
10	61.5	13.6	16.4	2.9	2.3	1.1	0.7

Fig. 5. SEM images of MS pastes immersed in 0.1 M HCl for 90 d. EDX data expressed as normalised atom %. The images illustrate (a) areas not attacked by acid, (b) areas attacked by acid and (c) an Al-based decomposition product.

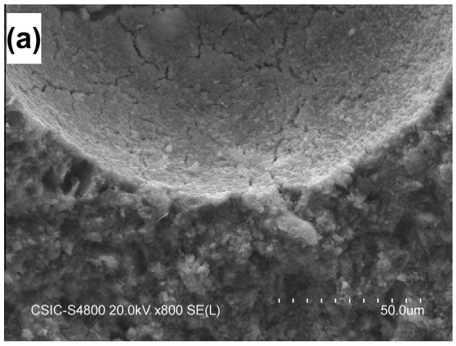

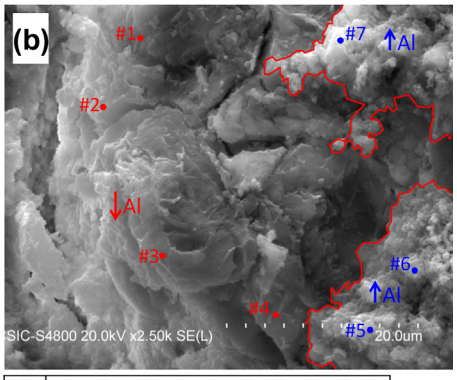

Point	O	Ca	Si	Al	S	K	Na	Mg	Cl	Fe
1	65.8	0.3	31.2	1.1	0.1	0.1	0.1	0.1	0.6	0.5
2	65.3	0.3	29.6	2.2	0.1	0.2	0.3	0.4	0.5	0.8
3	65.5	0.3	30.1	1.9	0.1	0.1	0.2	0.3	0.4	0.8
4	65	0.3	28.9	1.1	0	0	0	0	0.4	3.3
5	63.5	0.4	23.1	8.2	0.1	0.7	0.8	1.5	0.1	1.3
6	63.2	0.5	21.0	10.9	0.1	0.8	0.6	1.3	0.1	1.3
7	63.9	0.3	22.9	4.2	0.6	0.4	0.9	1.2	0.6	3.1

- Pores empty (no ettringite).
- Low [Ca] everywhere (<1%).
- Dealuminated gel zones - red points in b).
- Smooth morphology in Al poor gel .
- Nodular and irregular morphology in Al rich gel.

Fig. 6. SEM images of FAN-4 paste immersed in 0.1 M HCl for 90 d.

contrast, Fig. 5b shows a pore containing gels which have low Ca:Si ratios and considerably high Al contents. Point #9 appears to represent an amorphous silica gel. A number of globular precipitates were also noted in this pore which, according to EDX point 10, were aluminosilicate precipitates with minor levels of Ca, S and Fe. Finally, in Fig. 5c, a striking image of an amorphous Al precipitate is observed. This phase could be considered to be ettringite decomposition products and could be a combination of amorphous gibbsite type product ($Al(OH)_3$) and $Al_2(SO_4)_3$. Although the formation of Friedeĺs salt was indicated by XRD data, this phase was not observed in SEM-EDX analysis of the HCl-attacked MS pastes.

According to XRD data, all portlandite and ettringite present in FAN-4 pastes disappeared following acid immersion. The lack of ettringite in acid immersed FAN-4 pastes is illustrated by comparing Fig. 5a with Fig. 6a. In Fig. 6b, a clear distinction in gel morphology can be seen. The gels with smooth surfaces were basically silica gels arising from some type of acid-mediated decalcification–dealumination process. The gels with an irregular and nodular morphology (highlighted on the right hand side of Fig. 6b, were notably richer in Al and were either more resistant to acid attack or had not yet been attacked to the same degree. In general, the entire FAN-4 paste microstructure was poor in Ca, with no single EDX analysis registering more than 1% Ca. Possible reasons for the differences in paste microstructures in MS and FAN-4 pastes will be discussed later.

3.3. Effect of Na_2SO_4 solution and seawater on paste chemistry

Mortars based on both MS and FAN-4 cements maintained their original 28 d compressive strength and in many cases gained strength during immersion in 4.4% Na_2SO_4 solution or ASTM

seawater. Despite the lack of physical deterioration, it is necessary to investigate if any significant chemical changes took place in paste samples during immersion. Fig. 7 summarizes XRD data for pastes before and after 90 d immersion in Na_2SO_4 or seawater solutions.

Immersion of both pastes in 4.4% Na_2SO_4 solution had no appreciable effect on crystalline phase composition. Portlandite, ettringite, calcite and fly ash crystalline phase peaks were all relatively unchanged. However, when immersed in the ASTM seawater, some changes were noted particularly in the 9–15° 2Θ region of diffractograms for both pastes. In the control MS paste, the formation of Friedelśsalt (*F*) was apparent due to a new peak at 11.2°. In the FAN-4 pastes, the formation of a small amount of crystalline gypsum (*G*) was noted with the peak at 11.7°. To determine if these new crystalline phases are detectable by FTIR, spectra of the pastes before and after immersion in both Na_2SO_4 and seawater solution are included in Fig. 8.

The subtle changes observed in XRD data following seawater immersion for MS (Friedeĺs salt formation) and FAN-4 (small amount of gypsum formation) are difficult to confirm with the FTIR data in Fig. 8. The main absorption bands for Friedeĺs salt and gypsum are highlighted on the respective spectra where they are expected to appear. While there is some evidence of a slightly enhanced absorption at 786 cm^{-1} in the MS paste submerged in seawater, there is little evidence to corroborate gypsum formation in 90 d seawater-immersed FAN-4 pastes.

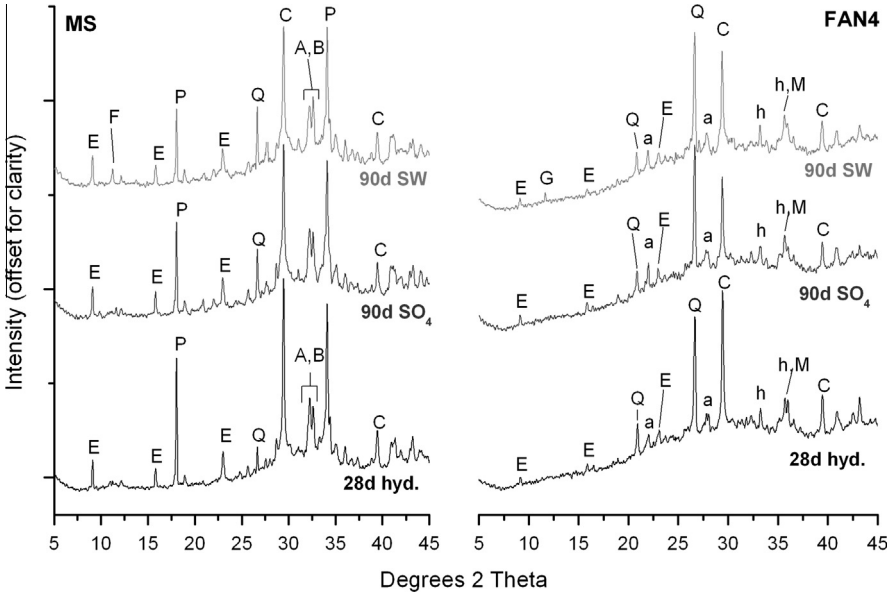

Fig. 7. XRD data for MS and FAN-4 pastes before and after immersion in either 4.4% Na_2SO_4 solution (SO_4) or ASTM seawater (SW) for 90 d.

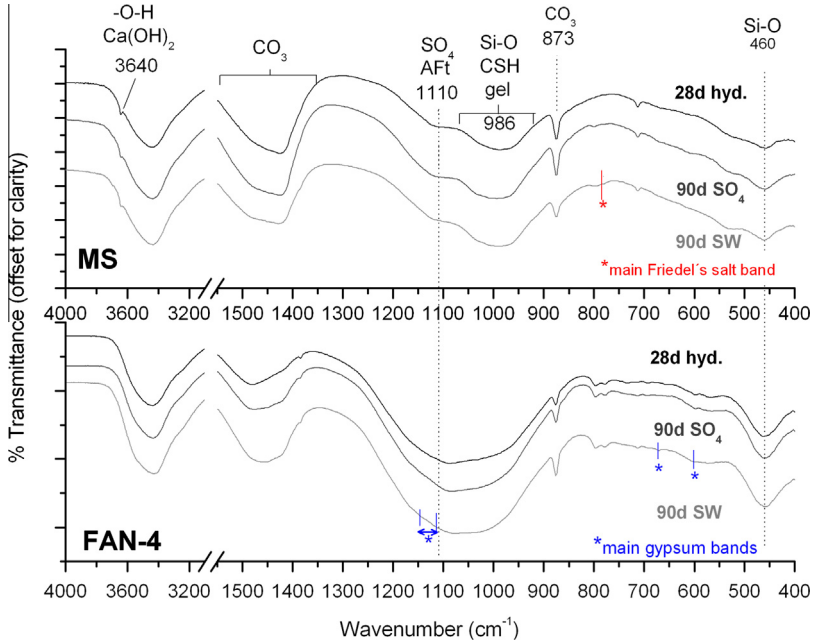

Fig. 8. FTIR data of MS and FAN-4 cement pastes before and after immersion in 4.4% Na_2SO_4 solution or ASTM seawater for 90 d.

4. Discussion

Given the strongly acidic nature of a 0.1 M HCl solution and the alkaline nature of Portland cement pastes, an obvious acid–base type reaction can be expected. The large losses in compressive strengths observed in Fig. 1 were due to the dissolution of cementitious gels in both MS and FAN-4 mortars. Before discussing possible acid attack mechanisms, it is first necessary to mention the nature of alkaline compounds present and likely cementitious gel structures in both systems.

4.1. Alkaline phases in MS and FAN-4 systems

Acid attack (with HCl) results in the dissolution of Ca containing phases such as $Ca(OH)_2$ and $CaCO_3$ as shown in the following equations: (2) and (3).

$$Ca(OH)_2 + 2HCl_{(aq)} \rightarrow CaCl_{2(aq)} + 2H_2O_{(l)} \quad (2)$$

$$CaCO_{3(s)} + 2HCl_{(aq)} \rightarrow CaCl_{2(aq)} + H_2CO_{3(aq)} \leftrightarrow H_2O_{(l)} + CO_{2(g)} \quad (3)$$

The presence of $Ca(OH)_2$ and $CaCO_3$ was much higher in MS pastes and these phases can be considered as an "acid buffer" of sorts, which would help explain the higher initial acid resistance of MS mortars shown in Fig. 1. The alkali in the FAN-4 system is instead dominated by NaOH and will be at least partially consumed by reaction with fly ash glassy phases. Unlike $Ca(OH)_2$ and its carbonation product $CaCO_3$, both NaOH and Na_2CO_3 are highly soluble in water. Although both the Na compounds can be considered to provide a reasonable degree of acid buffering capacity for the FAN-4 system, the fact that they are soluble and that HCl immersion solutions were changed on a number of occasions means that these Na-based acid buffering compounds were effectively removed from the system to a much greater degree than their Ca equivalents, which are only sparingly soluble.

Acid attack is generally a progressive reaction, where the degradation process proceeds gradually inwards. In areas where portlandite and calcite (or $NaOH/Na_2CO_3$) contents become depleted, the Ca in cementitious gels can be easily removed, resulting in a loss of their cementitious properties (strength).

Another difference between the MS and FAN-4 cements was the much higher quantity of ettringite (AFt) present in hydrated MS pastes. In these pastes, XRD data showed that AFt decomposed to a mixture of monosulfate (AFm) and Friedeĺs salt. A similar process may occur in the FAN-4 pastes, but was not detected due to their much lower initial content of AFt. Potential reaction mechanisms are given in Eqs. (4) and (5), where AFm could be identified as an intermediate product.

$$3CaO \cdot Al_2O_3 \cdot 3CaSO_4 \cdot 32H_2O + 4HCl \rightarrow 3CaO \cdot Al_2O_3 \cdot CaSO_4 \cdot 10H_2O + 2CaCl_2 + 2H_2SO_4 \quad (4)$$

$$3CaO \cdot Al_2O_3 \cdot CaSO_4 \cdot 10H_2O + 6HCl \rightarrow 3CaO \cdot Al_2O_3 \cdot CaCl_2 \cdot 10H_2O + 3H_2SO_4 \quad (5)$$

4.2. Nature of cementitious gels in the MS and FAN-4 systems

Data for MS pastes imply that the gel can be considered to be a typical C-S-H gel formed by PC hydration. The structure of such gels was originally described by Taylor and has since been extensively studied [22,29,42–44]. It consists of a planar, sandwich type structure with two imperfect layers of silicate tetrahedra joined by a central layer of octahedrally coordinated Ca. The typical Ca:Si ratio of C-S-H gels from PC hydration is around 1.5. Such gels have structures that resemble the imperfect "dreirkette" structures found in tobermorite [29].

Based on data previously produced by the authors, the gel structure in the FAN4 paste is significantly different. The Ca content of the system is much lower as a direct consequence of the lower clinker content and higher class F fly ash content. The presence of soluble Na^+ is considered to promote the alkali dissolution of Si and Al from fly ash glassy phases and lead to the formation of gels with a higher Al content and a lower Ca:Si ratio [28]. As yet unpublished ^{29}Si NMR data revealed that the gel in these FAN-4 pastes is highly polymerized. This was considered by the authors to be due to bridging of incomplete silicate chains with soluble Al or Si provided by fly ash. Where Al^{3+} is present in a tetrahedral co-ordination, it will carry a negative charge which can be satisfied by interlayer cations such as Na^+. This type of arrangement has been previously postulated to exist in pure alkali activated fly ash cements [25,45–47].

The two main differences in the gel systems are therefore:

1. Much lower Ca:Si ratio in FAN-4 pastes.
2. Higher Al content content in FAN-4 pastes.

Decalcification [48,49] and dealumination [50,51] processes for cementitious gels have been previously described in the literature. The dealumination process via acid treatment is of particular interest in the zeolite industry [52,53]. Even with alkali activated fly ash cements, the end product of either process is the same, an amorphous silica gel which contributes to the XRD background halo [50,54,55]. Such a product fits perfectly well with the FTIR absorption band at 1201 cm^{-1} observed in Figs. 3 and 4 for both pastes.

In the MS pastes, a standard decalcification process occurs in acid attacked gels. A number of Al-rich decomposition products were noticed in Fig. 5. One example was very high Al content precipitates containing some SO_4. These are likely to be amorphous gibbsite type products formed from ettringite decomposition. Where dissolved Al comes into contact with dissolved silicate species, a globular aluminosilicate precipitate is observed in the MS pastes. The dealumination process taking place in the FAN-4 pastes is clearly highlighted in the SEM/EDX data in Fig. 6b. Dealumination in these pastes may be occurring due to both the fact that much less Ca was generally present in the first place and that Al formed a greater part of the cementitious gel component than in the MS pastes.

Nonetheless, over the longer term, no significant difference in the intrinsic acid resistance of the FAN-4 and MS pastes was evident based on residual compressive strengths or final decomposition products (silica gel).

4.3. Resistance to sulfate attack

Both MS and FAN-4 cements showed a satisfactory performance during immersion in Na_2SO_4 solution. Sulfate degradation mechanisms involve reaction with portlandite or AFm. The substantially higher C_3A content in the MS pastes should in theory make it more susceptible to sulfate attack. However, other factors such as Fe_2O_3, C_4AF content, alkali content and cement powder specific surface area have been found to be important and a clear relationship exists between sulfate resistance and water to binder ratio [56–59].

Instead, the results in Fig. 1 revealed strength gains in both MS and FAN-4 mortars, which may be a result of dissolution and regrowth of more extensive ettringite crystals in the pore network, thus densifying the microstructure. Such a phenomenon can be described as "Ostwald ripening", where small crystals of high surface energy have a thermodynamic tendency to grow and thus reduce their effective surface area [60]. Thus, the most favourable sites for crystal growth are in macro-pores.

4.4. Seawater resistance

While the chemical degradation mechanisms in seawater also involve expansive sulfate mediated reactions such as portlandite → gypsum and AFm → AFt, the high Cl^- content is also important. It is widely regarded that Cl^- ions have a mitigating effect on sulfate attack mechanisms by conversion of AFm (and possibly AFt phases) to the insoluble Friedel's salt, effectively competing with SO_4^{2-} for AFm phases and preventing the expansive SO_4^{2-}-mediated formation of AFt [61–65]. According to Glasser et al., [66], AFm phases can be converted to Kuzel's salt in the presence of SO_4^{2-} and Cl^- or Friedel's salt in the presence of Cl^-. The XRD data for MS pastes in Figs. 3 and 7 show the formation of Friedel's salt after both seawater and HCl immersion, suggesting that this process is not very sensitive to pH. In the case of FAN-4 pastes, initial C_3A and thus ettringite and AFm contents were so low that appreciable changes were not detected. The only change of note was the formation of a small amount of a gypsum precipitate in Fig. 7.

In work with pure phases, Gabrisova et al. [67] showed that upon adding H_2SO_4 to reduce the system pH < 10, ettringite and monosulfate converted to gypsum and aluminium sulfate. The XRD evidence presented for MS pastes suggest that in acidic pH environments, an AFt → AFm → Friedel's salt process occurred, whereas in the higher pH environment and in the presence of high quantities of SO_4^{2-} and Cl^- ions, Friedel's salt was also formed but no AFm. Both the higher pH and SO_4^{2-} content of seawater are likely to be important in preventing the conversion of AFt to AFm. Regardless, the compressive strength data for both FAN-4 and MS pastes indicate that they present adequate resistance to sea water degradation mechanisms over the period studied.

5. Conclusions

This work has attempted to evaluate the resistance of a very high volume fly ash cement activated by Na_2SO_4 to immersion in various aggressive solutions. Following comparison with a commercially available sulfate resistant cement, the following conclusions can be drawn from the results presented:

- Overall, the novel FAN-4 binder presented satisfactory resistance to the aggressive solutions studied here when compared to a commercially available sulfate resistant cement reference.
- Both sets of mortars demonstrated adequate resistance to immersion in a 4.4% Na_2SO_4 solution and in ASTM seawater for periods up to 90 d.
- The higher content of AFt in reference MS pastes allowed the partial conversion of AFt to Friedel's salt to be observed in Cl^- rich environments. In seawater, the conversion process appears to be AFt → Friedels salt whereas in HCl, AFm was also observed, perhaps as an intermediate product.
- The MS paste presented a higher initial acid resistance than the FAN-4 paste. This has been explained by the presence of high quantities of $Ca(OH)_2$ and $CaCO_3$ phases, which act as useful acid buffers. Even after 90 d immersion in 0.1 M HCl, ettringite and portlandite could still be observed in internal parts of the MS paste specimens when examined by XRD and SEM/EDX. Alternatively, in the FAN-4 pastes, no portlandite was present to begin with and the main alkali sources are expected to be $NaOH/Na_2CO_3$, which are highly soluble and can be effectively removed when changing acid solutions.
- Both pastes showed characteristic signs of acid attack on cementitious gel structures. The emergence of a halo around 20–25° 2Θ in MS paste XRD data and from 18° to 28° 2Θ in FAN-4 paste coincided with a new FTIR absorption band at about 1200 cm^{-1}, typical of colloidal silica gel.
- In MS pastes, a decalcification process during acid attack of gels and the release of Al from ettringite is envisaged. Due to the lower Ca content and higher Al content in FAN-4 cementitious gels, a slight decalcification process and a major dealumination process are hypothesised based on SEM/EDX observations.

Acknowledgements

The authors are very grateful for the financial support that allowed this work to be carried out via the award of a JAE Post-Doc scholarship to Shane Donatello, co-funded by the Spanish Ministerio de Ciencia e Innovación and the European Social Fund and also to a research grant awarded to Ana Fernandez (BIA 2010 17530) by the Minesterio de Ciencia e Innovación.

References

[1] Emmons PH, Sordyl DJ. The state of the concrete repair industry, and a vision for its future. Concr. Repair Bull. 2006(July/August).
[2] Swamy RN. The alkali–silica reaction in concrete. Glasgow: Blackie and son; 1992.
[3] Garcia-Lodeiro I, Palomo A, Fernandez-Jimenez A. Alkali-aggregate reaction in activated fly ash systems. Cem Concr Res 2007;37(2):175–83.
[4] Gadea J, Soriano J, Martin A, Campos PL, Rodriguez A, Junco C, et al. The alkali-aggregate reaction for various aggregates used in concrete. Mater Constr 2010;60(299):69–78.
[5] Massazza F. Pozzolanic cements. Cem Concr Comp 1993;15(4):185–214.
[6] Baghabra Al-Amoudi OS, Maslehuddin M, Ibrahim M, Shameem M, Al-Methel MH. Performance of blended cement concretes prepared with constant workability. Cem Concr Comp 2011;33(1):90–102.
[7] Badogiannis E, Tsivilis S. Exploitation of poor Greek kaolins: durability of metakaolin concrete. Cem Concr Comp 2009;31(2):128–33.
[8] Rodriguez de Sensale G. Effect of rice-husk ash on durability of cementitious materials. Cem Concr Comp 2010;32(9):718–25.
[9] Flatt RJ, Roussel N, Cheeseman CR. Concrete: an eco-material that needs to be improved. J Eur Ceram Soc 2012;32:2787–98.
[10] EN 197-1. Part 1; Composition, specifications and conformity criteria for common cements 2000.
[11] Malhotra VM. Durability of concrete incorporating high-volume of low-Calcium (ASTM Class F) fly ash. Cem Concr Comp 1990;12(4):271–7.
[12] Lam L, Wong YL, Poon CS. Degree of hydration and gel/space ratio of high-volume fly ash/cement systems. Cem Concr Res 2000;30:747–56.
[13] Bouzoubaa N, Zhang MH, Malhotra VM. Laboratory-produced high-volume fly ash blended cements: compressive strength and resistance to the chloride-ion penetration of concrete. Cem Concr Res 2000;30:1037–46.
[14] Bentz DP, Sato T, de la Varga I, Weiss WJ. Fine limestone additions to regulate setting in high volume fly ash mixtures. Cem Concr Comp 2012;34:11–7.
[15] Bentz DP. Powder additions to mitígate retardation in high-volume fly ash mixtures. ACI Mat J 2010;107(5):508–14.
[16] De Weerdt K, Haha MB, Le Saout G, Kjellsen KO, Justnes H, Lottenbach B. Hydration mechanisms of ternary Portland cements containing limestone powder and fly ash. Cem Concr Res 2011;41(3):279–91.
[17] De Weert K, Kjellsen KO, Sellevold E, Justnes H. Synergy between fly ash and limestone powder in ternary cements. Cem Concr Comp 2011;33(1):30–8.
[18] Kumar S, Kumar R, Bandopadhyay A, Alex TC, Kumar BR, Das SK, et al. Mechanical activation of granulated blast furnace slag and its effect on the properties and structure of Portland slag cement. Cem Concr Comp 2008;30(8):679–85.
[19] Kolani B, Buffo-Lacarriere L, Sellier A, Escadeillas G, Boutillon L, Linger L. Hydration of slag-blended cements. Cem Concr Comp 2012;34(9):1009–18.
[20] Palomo A, Fernandez-Jimenez A, Kovalchuk G, Ordonez LM, Naranjo MC. OPC-fly ash cementitious systems: study of gel binders produced during alkaline hydration. J Mater Sci 2007;42(9):2958–66.
[21] Shi C, Day RL. Acceleration of the reactivity of fly ash by chemical activation. Cem Concr Res 1995;25(1):15–21.
[22] Richardson IG. The nature of C–S–H in hardened cements. Cem Concr Res 1999;29:1131–47.
[23] Renaudin G, Russias J, Leroux F, Cau-dit-Cournes C, Frizon F. Structural characterization of C–S–H and C–AS–H samples – Part II: Local environment investigated by spectroscopic analyses. J Solid State Chem 2009;182(12):3320–9.
[24] Puertas F, Palacios M, Manzano H, Dolado JS, Rico A, Rodriguez J. A model for the C–A–S–H gel formed in alkali-activated slag cements. J. Eur Ceram Soc 2011;31(12):2043–56.
[25] Palomo A, Alonso S, Fernández-Jiménez A, Sobrados I, Sanz J. Alkali activation of fly ashes: NMR study of the reaction products. J Am Ceram Soc 2004;87:1141–5.
[26] Yip CK, Lukey GC, Van Deventer JSJ. The coexistence of geopolymeric gel and calcium silicate hydrate at the early stage of alkaline activation. Cem Concr Res 2005;35(9):1688–97.

[27] Garcia-Lodeiro I, Palomo A, Fernandez-Jimenez A, MacPhee DE. Compatibility studies between N–A–S–H and C–A–S–H gels. study in the ternary diagram Na_2O–CaO–Al_2O_3–SiO_2–H_2O. Cem Concr Res 2011;41(9):923–31.
[28] Donatello S, Fernandez-Jimenez A, Palomo A. Very high volume fly ash cements. Early age hydration study using Na_2SO_4 as an activator. J Am Ceram Soc <http://dx.doi.org/10.1111/jace.12178>.
[29] Taylor HFW. Cement Chemistry. 2nd ed. London: Thomas; 1997.
[30] Hewlett PC, editor. Leás Chemistry of cement and concrete. London: Elsevier; 2004.
[31] EN 1015-3, Methods of test for mortar for masonry – Part 3: Determination of consistence of fresh mortar (by flow table) 1999.
[32] EN 196-1 Methods of testing cement – Part 1: Determination of strength 2005.
[33] ASTM D1141, Standard Practice for the Preparation of Substitute Ocean Water 2008.
[34] Measurement of the leachability of solidified low-level radioactive wastes by a short term test procedure. ANSI/ANS 16.1. American Nuclear Society, La Grange Park, II, 1986.
[35] Talero R, Trusilewicz L, Delgado A, Pedrajas C, Lannegrand R, Rahhal V, et al. Comparative and semi-quantitative XRD analysis of Friedeĺs salt originating from pozzolan and Portland cement. Const Buil Mater 2011;25:2370–80.
[36] Baur I, Keller P, Mavrocordatos D, Wehrli B, Annette Johnson C. Dissolution-precipitation behaviour of ettringite–monosulfate and calcium silicate hydrate. Cem Concr Res 2004;34:341–8.
[37] Hirao H, Yamada K, Takahashi H, Zibara H. Chloride binding of cement estimated by binding isotherms of hydrates. J Adv Concr Technol 2005;3(1):77–84.
[38] Calabro DC, Valyocsik EW, Ryan FX. In situ ATR/FTIR study of mesoporous silicate syntheses. Microporous Mater 1996;7(5):243–59.
[39] Zeglinski J, Piotrowski GP, Piekos R. A study of interaction between hydrogen peroxide and silica gel by FTIR spectroscopy and quantum chemistry. J Mol Struct 2006;794:83–91.
[40] Cai Y, Xue J, Polya DA. A fourier transform infrared spectroscopic study of Mg-rich, Mg-poor and acid leached palygorskites. Spectrochim Acta A 2007;66(2):282–8.
[41] Pajares I, Martinez-Ramirez S, Blanco-Varela MT. Evolution of ettringite in presence of carbonate and silicate ions. Cem Concr Comp 2003;25:861–5.
[42] Taylor HFW. Nanostructure of C–S–H: current status. Adv Cem Based Mater 1993;1(1):38–46.
[43] Cong X, Kirkpatrick RJ. ^{29}Si MAS NMR study of the structure of Calcium silicate hydrate. Adv Cem Based Mater 1996;3:144–56.
[44] García-Lodeiro I, Fernández-Jiménez A, Sobrados I, Sanz J, Palomo A. C–S–H gels: interpretation of ^{29}Si MAS-NMR spectra. J Am Ceram Soc 2012;5(4):1440–6.
[45] Palomo A, Grutzeck MW, Blanco MT. Alkali-activated fly ashes. A cement for the future. Cem Concr Res 1999;29:1323–9.
[46] Fernández-Jiménez A, Palomo A. Mid-infrared spectroscopic studies of alkali-activated fly ash structure. Micropor Mesopor Mat 2005;86:207–14.
[47] Duxson P, Fernández-Jiménez A, Provis JL, Lukey GC, Palomo A, van Deventer JSJ. Geopolymer technology: the current state of the art. J Mater Sci 2007;42:2917–33.
[48] Kurdowski W. The protective layer and decalcification of C-S-H in the mechanism of chloride corrosion of cement paste. Cem Concr Res 2004;34:1555–9.
[49] Puertas F, Goñi S, Hernández MS, Varga C, Guerrero A. Comparative study of accelerated decalcification process among C_3S grey and White cement pastes. Cem Concr Comp 2012;34:384–91.
[50] Allahverdi A, Skvara F. Nitric acid attack on hardened paste of geopolymeric cements. Part I. Ceram–Silikaty 2001;45(3):81–8.
[51] Allahverdi A, Skvara F. Sulfuric acid attack on hardened paste of geopolymer cements. Part I. Mechanism of corrosion at relatively high concentrations. Ceram–Silikaty 2005;49(4):225–9.
[52] Baran R, Millot Y, Onfroy T, Krafft J-M, Dzwigaj S. Influence of the nitric acid treatment on Al removal, framework composition and acidity of BEA zeolite investigated by XRD, FTIR and NMR. Micropor Mesopor Mater 2012;163:122–30.
[53] Yue MB, Xue T, Jiao WQ, Wang YM, He MY. Dealumination, silicon insertion and H-proton exchange of NaY in one step with acid ethanol solution. Micropor Mesopor Mat 2012;159:50–6.
[54] Bakharev T. Resistance of geopolymer materials to acid attack. Cem Concr Res 2005;35:658–70.
[55] Fernández-Jiménez A, García-Lodeiro I, Palomo A. Durability of alkali-activated fly ash cementitious materials. J Mater Sci 2007;42:3055–65.
[56] Talero R, Palacios J. Influence of the parameter "specific surface" in the quantification as high, or not, sulphate resistance of a Portland cement. Cem Concr Res 1993;23:1237–44.
[57] Tikalsky PJ, Roy D, Scheetz B, Krize T. Redefining cement characteristics for sulphate resistant Portland cement. Cem Concr Res 2002;32(8):1239–46.
[58] Boyd AJ, Mindess S. The use of tension testing to investigate the effect of W/C ratio and cement type on the resistance of concrete to sulphate attack. Cem Concr Res 2004;34(3):373–7.
[59] Sahmaran M, Kasap O, Duru K, Yaman IO. Effects of mix composition and water-cement ratio on the sulfate resistance of blended cements. Cem Concr Comp 2007;29(3):159–67.
[60] Skalny J, Johansen V, Thaulow N, Palomo A. DEF: As a form of sulphate attack. Mater Constr 1996;46(244):5–29.
[61] Ben-Yair M. The durability of cement and concrete in sea water. Desalination 1967;3:147–54.
[62] Rasheeduzzafar, Al-Saadoun SS, Al-Gahtani AS, Dakhil FH. Effect of tricalcium aluminate content of cement on corrosion of reinforcing steel in concrete. Cem Concr Res 1990;20(5):723–38.
[63] Al-Amoudi OSB, Maslehuddin M, Abdul-Al YAB. Role of chloride ions on expansion and strength reduction in plain and blended cements in sulphate environments. Constr Build Mater 1995;9(1):25–33.
[64] Santhanam M, Cohen M, Olek J. Differentiating seawater and groundwater sulphate attack in Portland cement mortars. Cem Concr Res 2006;36(2):2132–7.
[65] Zhang M, Chen J, Lv Y, Wang D, Ye J. Study on the expansion of concrete under attack of sulphate and sulphate–chloride ions. Constr Build Mater 2013;39:26–32.
[66] Glasser FP, Kindness A, Stronach SA. Stability and solubility relationships in AFm phases. Part I. Chloride, sulphate and hydroxide. Cem Concr Res 1999;29:861–6.
[67] Gabrisova A, Havlica J, Sahu S. Stability of calcium sulphoaluminate hydrates in water solutions with various pH values. Cem Concr Res 1991;21:1023–7.